Lattice dynamics in austenitic stainless steels Fe–18Cr–12Ni–2Mo and Fe–18Cr–16Ni–10Mn

2004 J. Phys.: Condens. Matter 16 2609

(http://iopscience.iop.org/0953-8984/16/15/012)

INSTITUTE OF PHYSICS PUBLISHING JOURNAL OF PHYSICS: CONDENSED MATTER

J. Phys.: Condens. Matter **16** (2004) 2609–2616 PII: S0953-8984(04)73703-0

Lattice dynamics in austenitic stainless steels Fe–18Cr–12Ni–2Mo and Fe–18Cr–16Ni–10Mn

V Rajevac[1,5], M Hoelzel[1], S A Danilkin[2], A Hoser[3,4] and H Fuess[1]

[1] Darmstadt University of Technology, Institute for Materials Science, Petersenstraße 23, D-64287 Darmstadt, Germany
[2] Hahn-Meitner-Institut, SF2, Glienicker Straße 100, D-14109 Berlin, Germany
[3] Forschungszentrum Jülich, IFF, D-52425 Jülich, Germany
[4] RWTH Aachen, D-52056 Aachen, Germany

Received 17 December 2003
Published 2 April 2004
Online at stacks.iop.org/JPhysCM/16/2609
DOI: 10.1088/0953-8984/16/15/012

Abstract

Phonon dispersion curves of austenitic stainless steels Fe–18Cr–16Ni–10Mn and Fe–18Cr–12Ni–2Mo have been measured by triple-axis neutron spectroscopy. The data were analysed using Born–von Karman interactions as well as calculations including the contribution of conduction electrons on the lattice dynamics. An appropriate description of the experimental data was obtained by taking into account two-neighbour shells plus the contribution of the electron gas. The elastic constants and moduli obtained are close to reported results by ultrasonic studies on polycrystalline samples. The phonon densities of states in both systems calculated from the dispersion curves agree well with results obtained by time-of-flight neutron spectroscopy on polycrystalline samples. The Debye temperature $\Theta(T)$ shows a minimum around 40 K, similar to copper and nickel.

1. Introduction

Austenitic stainless steels are widely applied because they combine high corrosion resistance with good mechanical and physical properties. These properties can be tuned by variation of the composition of the main elements Fe, Cr and Ni, by adding further alloying elements and also by changes in their microstructure due to thermal and mechanical treatment. To design a steel for a distinct application, a prediction of its properties based on its chemical composition would be supportive. The effects of alloying additions on the engineering elastic moduli of austenitic stainless steels have been investigated by ultrasonic measurements [1–3] and inelastic neutron scattering [4]. As an example, it was found that adding Ni as well as Cr (both as substitute for Fe) leads to an increase in the bulk modulus accompanied by a decrease in the shear modulus [3]. These results contradict predictions based on the theory

[5] Author to whom any correspondence should be addressed.

of elasticity, as substituting Fe with Cr leads to lattice expansion while substituting Fe with Ni decreases the lattice parameter. Furthermore, it is remarkable that the bulk modulus and the shear modulus change in opposite directions. These results indicate significant changes in the interatomic bonding due to modifications in the chemical composition in such a way that dilatational modes and shear modes are affected in a quite different manner. Recently, the effects of alloying additions on the properties of austenitic stainless steels have been derived from *ab initio* quantum mechanical calculations [5].

Phonon dispersion curves are often used to verify interatomic potentials. Moreover, semi-empirical approaches, such as the embedded-atom method, require elastic constants and characteristic points in phonon dispersion curves among the parameters for the determination of interatomic potentials, from which the material properties can be derived.

In previous studies, the phonon dispersion branches L-[110] and T_1-[110] of Fe–18Cr–16Ni–10Mn steel, measured by time-of-flight neutron spectroscopy [6], and the low q regions of the phonon dispersion branches, measured by triple-axis neutron spectroscopy [7], have been presented. Also, the phonon dispersion branches of Fe–18Cr–12Ni–2Mo were measured along the symmetry directions [100], [110] and [111] [8]. In this study, we present measurements of the phonon dispersion branches and the vibrational frequency spectra of steels Fe–18Cr–16Ni–10Mn and Fe–18Cr–12Ni–2Mo as well as corresponding model calculations. The parameters of the model calculations have been used to derive elastic and thermal properties.

2. Experimental details

Single crystals of $15 \times 15 \times 25$ mm^3 (Fe–18Cr–12Ni–2Mo) and $8 \times 8 \times 40$ mm^3 (Fe–18Cr–16Ni–10Mn) were prepared by the Bridgman method at the Tomsk State University, Russia. The measurements of the dispersion branches were carried out at the triple-axis spectrometer UNIDAS at Forschungszentrum Jülich, Germany. For both steels a lattice parameter of 3.593(3) Å was obtained. The mosaic spread of the Fe–18Cr–12Ni–2Mo crystal was determined to be 40′, whereas in the sample of Fe–18Cr–16Ni–10Mn a mosaic spread of 30′ was found. All measurements of both steels were carried out in constant-Q mode using a fixed incident neutron energy of 14.74 meV. The measurements of the phonon density of states were performed at the time-of-flight spectrometer DIN-2PI at the JINR, Dubna, Russia. Polycrystalline plates of $10 \times 18 \times 65$ mm^3 (Fe–18Cr–16Ni–10Mn) and $2 \times 150 \times 150$ mm^3 (Fe–18Cr–12Ni–2Mo) were investigated using an incident neutron energy of 10.3 meV. The range of momentum transfer was $Q = 1.1$–4.1 Å^{-1} for elastic scattering. Neutron energy transfers $\hbar\omega$ from 4 to 60 meV were measured. The data were corrected with respect to background and detector efficiency.

3. Results and discussion

3.1. Phonon dispersion curves

The dispersion branches of Fe–18Cr–12Ni–2Mo and Fe–18Cr–16Ni–10Mn (figures 1 and 2) are similar to those of various other fcc metals and alloys. Fe–18Cr–12Ni–2Mo shows a slightly concave curvature in the T_1-[110] branch in the low q region. A similar behaviour was also observed in Ca [9], Yb [10], γ-Fe [11], $Fe_{0.7}Ni_{0.3}$ [12], and $Fe_{0.72}Pd_{0.28}$ [13]. This behaviour is however not visible in Fe–18Cr–16Ni–10Mn. A possible reason for a concave curvature in the T_1-[110] branch could be anharmonicity of the potential or electron–phonon interactions [9, 10]. Significant differences between Fe–18Cr–12Ni–2Mo and Fe–18Cr–16Ni–10Mn can be found in the L-[110] branches, where Fe–18Cr–12Ni–2Mo shows lower frequencies.

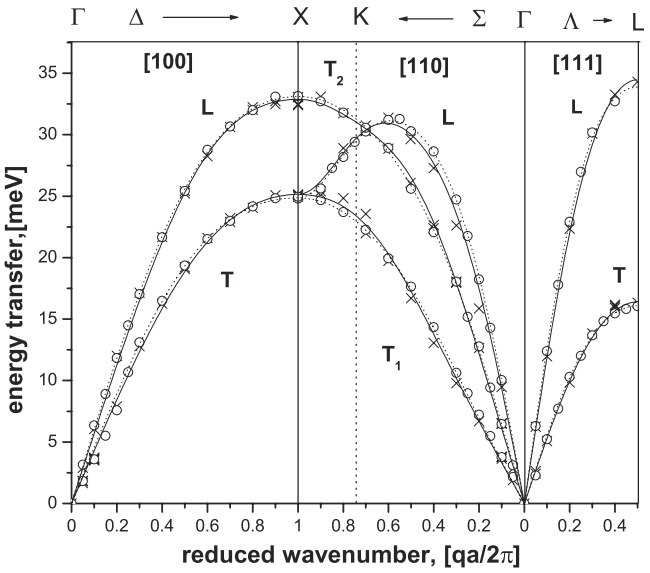

Figure 1. Measured phonon dispersion curves for Fe–18Cr–12Ni–2Mo (×), Fe–18Cr–16Ni–10Mn (○), calculations based on Born–von Karman model, five-neighbour shells, generalized force matrix, for Fe–18Cr–12Ni–2Mo (——) and Fe–18Cr–16Ni–10Mn (· · · · · ·).

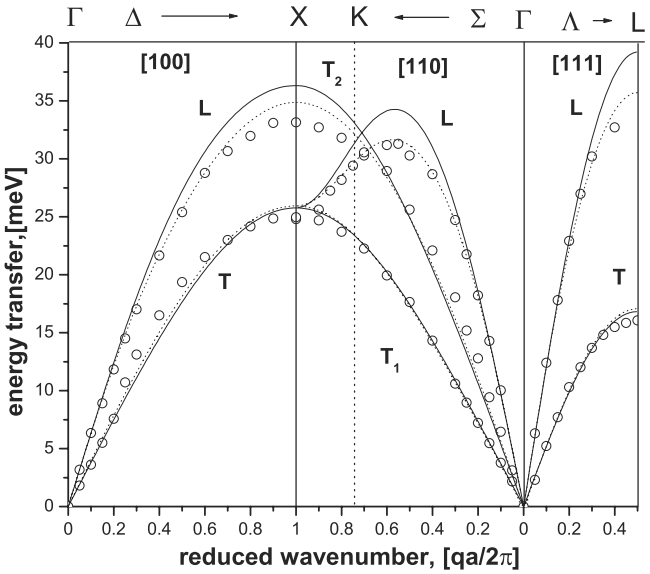

Figure 2. Measured phonon dispersion curves for Fe–18Cr–16Ni–10Mn (○), calculations based on Born–von Karman model, two-neighbour shells, generalized force matrix without (——) and with electron gas contribution (· · · · · ·).

The data were analysed by model calculations based on Born–von Karman interactions using generalized force matrices as well as the approximation of axial symmetrical interactions. The model calculations were carried out up to eight-neighbour shells. An adequate fit to the experimental points was obtained by including five-neighbour shells. Taking into account more neighbour shells did not lead to improvements in the description of the experimental data. Model calculations based on generalized force matrices gave better descriptions of the experimental results than calculations using the assumption of axial symmetrical interactions, especially for cases of only few-neighbour shells.

The elastic constants were derived from the interatomic force constants by expanding the components of the dynamical matrices in the low q limit. The polycrystalline elastic moduli

Table 1. Elastic properties in austenitic stainless steels.

	Fe–18Cr–12Ni–2Mo			Fe–18Cr–16Ni–10Mn		
	BvK 5 neigh.	Low q	Ultrasonic [15]	BvK 5 neigh.	Low q	Ultrasonic [3]
C_{11} (GPa)	195.7	195.3	206	221.8	199.4	206.8
C_{12} (GPa)	130.1	132.1	133	154.0	125.3	134.6
C_{44} (GPa)	111.0	107.9	119	125.4	101.6	114.7
G (GPa)	68.3	67.2	74.2	74.5	68.5	72.3
B (GPa)	152.0	153.2	157.3	176.6	150.0	158.7
E (GPa)	180.4	175.8	194.7	199.0	178.5	190.4
ν	0.30	0.31	0.29	0.31	0.30	0.30
C_{12}/C_{11}	0.665	0.676	0.647	0.694	0.628	0.651
A	3.38	3.41	3.27	3.70	2.74	3.18

B, G and E and the Poisson ration ν were calculated from the elastic constants. In cubic systems, the bulk modulus is given by

$$B = (C_{11} + 2C_{12})/3. \tag{1}$$

For the calculation of the shear modulus, the Hershey–Kröner–Eshelby averaging method [14] was applied:

$$G^3 + \alpha G^2 + \beta G + \gamma = 0 \tag{2}$$

where α, β and γ are equal to:

$$\alpha = \frac{5C_{11} + 4C_{12}}{8} \tag{3}$$

$$\beta = -\frac{C_{44}(7C_{11} - 4C_{12})}{8} \tag{4}$$

$$\gamma = -\frac{C_{44}(C_{11} - C_{12})(C_{11} + 2C_{12})}{8}. \tag{5}$$

Table 1 illustrates the elastic properties derived from the Born–von Karman model (generalized matrices) including five-neighbour shells. Results obtained from ultrasonic studies on polycrystalline samples are also included. The single crystal elastic constants of Fe–18Cr–16Ni–2Mo have been derived by Ledbetter from the polycrystalline elastic moduli, using two empirical relations for fcc Fe–Cr–Ni alloys: $C_{12}/C_{11} = 0.635$ and for Zener's elastic anisotropy ratio $A = 2C_{44}/(C_{11} - C_{12}) = 3.51$ [15]. The second column of table 1 shows the averaged values from his calculations. We also calculated the elastic moduli of Fe–18Cr–16Ni–10Mn using a relation presented by Kim *et al* [3], which describes the separate effects of alloying elements on the elastic moduli of Fe–Cr–Ni–Mn austenitic stainless steels. To our knowledge, no ultrasonic studies on single crystals of Fe–18Cr–12Ni–2Mo or Fe–18Cr–16Ni–10Mn have been reported so far.

The calculations using Born–von Karman models disclose the existence of long range interactions, supposedly related to conduction electrons. The effects of the conduction electrons can be described by screening of the Coulomb interactions between the metal ions. A description of the lattice dynamics of metals taking into account the effects of conduction electrons was introduced by Krebs [16] and applied for fcc metals using the Morse potential by Mohammed *et al* [17]. The elements of the dynamical matrix consist of two parts [17]:

$$D^{\mathrm{TOT}}_{\alpha\beta} = D^{\mathrm{i}}_{\alpha\beta} + D^{\mathrm{e}}_{\alpha\beta}.$$

The first part is due to Coulomb interactions between the metal ions. The second part corresponds to the screening effect of conduction electrons and is given by [17]. In these

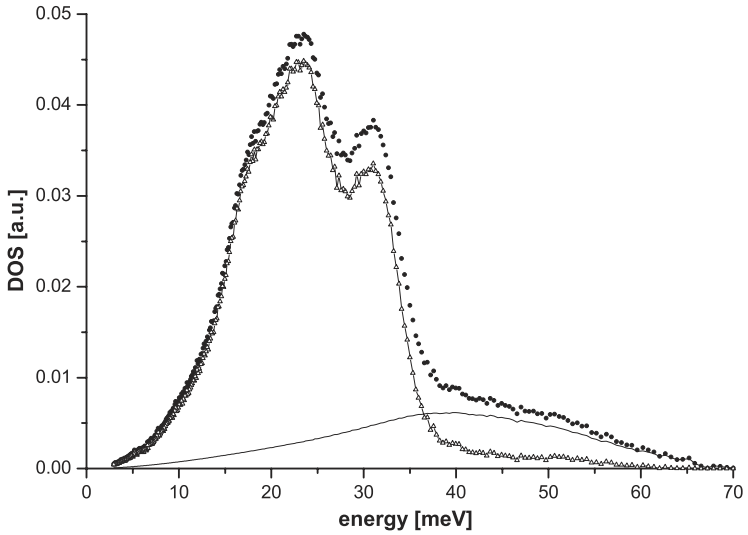

Figure 3. Vibrational density of states of steel Fe–18Ni–16Cr–10Mn: (●) experimental data, (——) multiphonon contribution, and (–△–) after multiphonon correction.

model calculations the discrete translation symmetry of the crystalline system is taken into account. The model contains the following assumptions: electrons are free fermions at $T = 0$ and the screened potential of atoms follows a Yukawa potential. The electronic term in the dynamical matrix introduces only one refineable parameter, $k_e = 18$–20 GPa, the bulk modulus of the electron gas [17]. From the general properties of electron gas a value of $k_c = 0.6455\ k_F = 0.700$ Å^{-1} was obtained. k_c was determined using a Thomas–Fermi approximation with an additional correction based on the many-body perturbation theory. From figure 2 it can be seen that for two-neighbour shells the insertion of electron gas terms in the components of the dynamical matrix leads to a significant improvement in the description of the experimental data compared to the conventional Born–von Karman model. Because of the long range Coulomb forces much fewer neighbour shells are required for an adequate fit to the experimental points. The improvement is especially pronounced in the regions close to the edges of the Brillouin zone in all directions. This effect is probably related to the screening of the Coulomb potential due to conduction electrons.

3.2. Frequency distribution spectra

The measured frequency distribution spectra for Fe–18Cr–12Ni–2Mo and Fe–18Cr–16Ni–10Mn are similar to those of other fcc systems, namely copper [18] and nickel [19]. The differences in the frequency spectra of both steels are in the range of the experimental errors. We used the method presented by Dawidowski *et al* [20, 21] for the calculation of multiphonon scattering contributions. Figures 3–5 present the vibrational density of states for both steels before and after subtraction of the multiphonon contribution. The vibrational density of states has also been derived from the modelling of the dispersion branches. The method of Gilat and Raubenheimer [22] was applied to the Born–von Karman model, generalized force matrices, including two-neighbour shells. The estimation on the error bars calculation which only include the statistical error show that differences between two phonon density of states are within the error bars. The results were convoluted with the resolution function of the spectrometer to enable a comparison with the data derived from the frequency spectra; see figure 6.

From the vibrational density of states the Debye temperature $\Theta(T)$ can be obtained. In further text Θ_D is the Debye temperature in the low temperature limit and Θ_∞ in the high

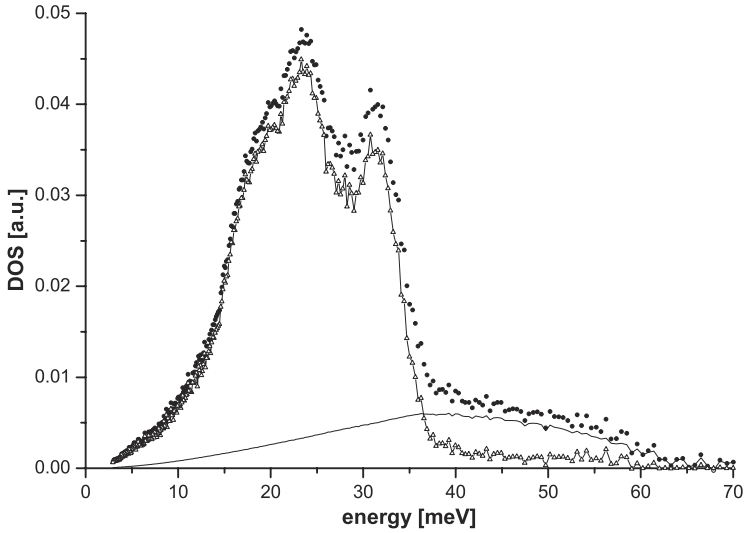

Figure 4. Vibrational density of states of steel Fe–18Ni–12Cr–2Mo: (●) experimental data, (——) multiphonon contribution, and (–△–) after multiphonon correction.

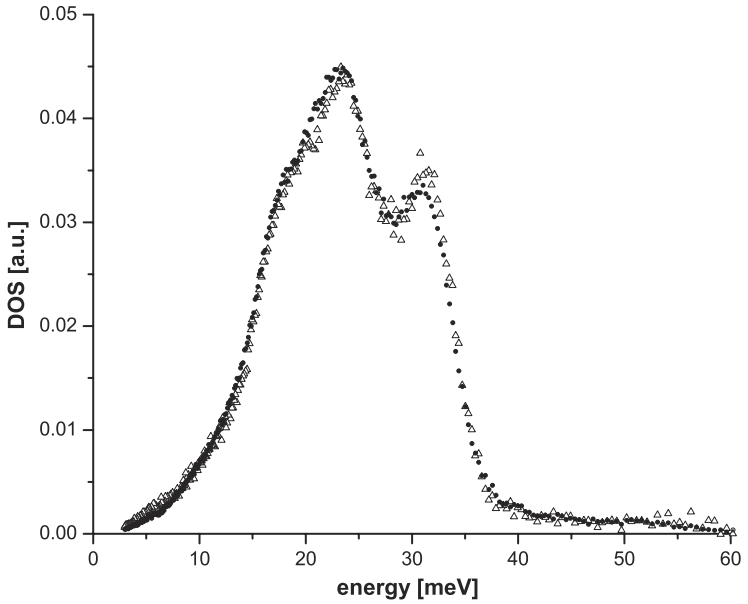

Figure 5. Vibrational density of states of steels: (●) Fe–18Cr–12Ni–2Mo, and (△) Fe–18Cr–16Ni–10Mn after multiphonon correction.

temperature limit, respectively. In equation (6) $x = \hbar\omega/kT$.

$$\int_0^{\omega_{\max}} \frac{(\frac{\hbar\omega}{kT})^2 \mathrm{e}^{\frac{\hbar\omega}{kT}}}{(\mathrm{e}^{\frac{\hbar\omega}{kT}} - 1)^2} g(\omega)\,\mathrm{d}\omega = 3\left(\frac{T}{\Theta}\right)^3 \int_0^{\Theta/T} \frac{x^4 \mathrm{e}^x}{(\mathrm{e}^x - 1)^2}\,\mathrm{d}x. \tag{6}$$

Expanding equation (6) to the low energy limit yields

$$g(\omega) = \frac{3\hbar^3\omega^2}{(k\Theta_{\mathrm{D}})^3}. \tag{7}$$

Applying equation (6) to our data on steels Fe–18Cr–16Ni–10Mn and Fe–18Cr–16Ni–2Mo reveals 406 and 410 K, respectively. These results are quite close to the Debye temperatures Θ_{D} for Fe–Cr–Ni alloys reported by Beskrovni *et al* [4]. The Debye temperature Θ_{D} is related

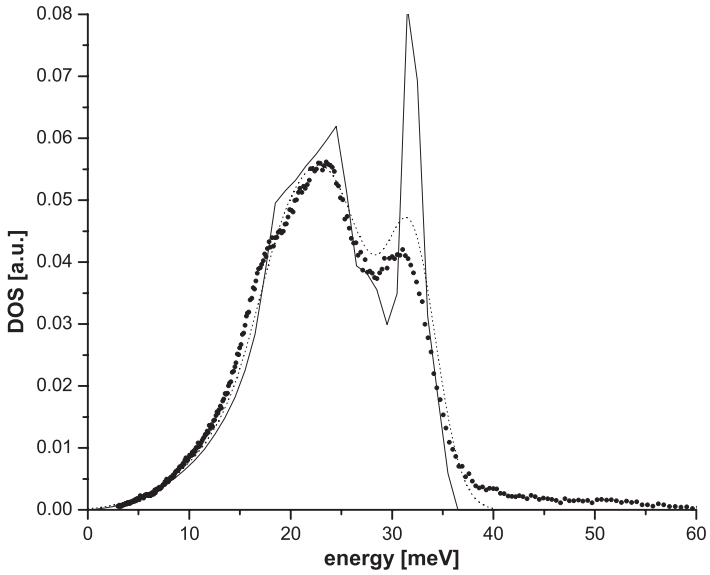

Figure 6. (●) Vibrational density of states of steel Fe–18Cr–16Ni–10Mn: (——) calculation using Born–von Karman model, generalized force matrices including two-neighbour shells, and (· · · · · ·) calculation using the same model after convolution with the instrumental resolution function.

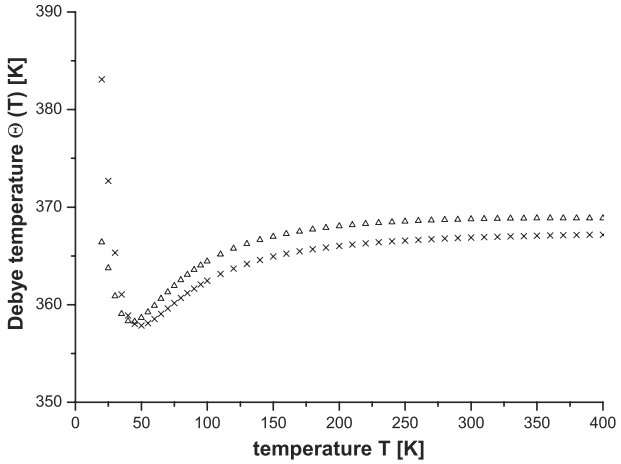

Figure 7. Debye temperature as a function of temperature for austenitic stainless steels: (×) Fe–18Cr–16Ni–10Mn, (△) Fe–18Cr–12Ni–2Mo.

to the velocities of sound in polycrystalline materials reported by [4]:

$$\Theta_{\mathrm{D}} = \frac{h}{k}\left(\frac{4\pi V}{9N}\right)^{-1/3}\left(\frac{1}{v_l^3}+\frac{2}{v_t^3}\right)^{-1/3}. \tag{8}$$

Using $G = \rho v_t^2$ and $B = \rho v_l^2 - \frac{4}{3}G$ [4] and our results for G and B presented in table 1 we obtain $\Theta_{\mathrm{D}} = 416$ K for Fe–18Cr–16Ni–10Mn and $\Theta_{\mathrm{D}} = 411$ K for Fe–18Cr–12Ni–2Mo, in satisfactory agreement with results obtained from the vibrational densities of states. In figure 7 the Debye temperature $\Theta(T)$ shows a minimum around 30–40 K for both steels. Similar minima positions have also been reported for copper [18] and nickel [19].

The specific heat capacities $C_V(T)$ of both steels were calculated from the vibrational densities of states by

$$C_V = k\int_0^{\omega_{\max}} \frac{(\frac{\hbar\omega}{kT})^2 \mathrm{e}^{\frac{\hbar\omega}{kT}}}{(\mathrm{e}^{\frac{\hbar\omega}{kT}}-1)^2} g(\omega)\,\mathrm{d}\omega. \tag{9}$$

The values of $C_V(T)$ obtained for both steels correspond to the Debye model.

4. Conclusions

Austenitic stainless steels Fe–18Cr–12Ni–2Mo and Fe–18Cr–16Ni–10Mn show very similar phonon dispersion curves which can be well described by model calculations including interactions of two-neighbour shells plus contributions of conduction electrons on the lattice dynamics. Our results for the elastic constants and engineering elastic moduli are close to results obtained by ultrasonic studies on polycrystalline samples. For further investigations of alloying effects on elastic constants and moduli, ultrasonic measurements on single crystals would be supportive. The calculations of vibrational densities of states from modelling of phonon dispersion branches were confirmed by measurements of the vibrational frequency spectra. Experimental data based on phonon density of states show that differences between two samples are inside error bars.

Acknowledgments

Financial support by the Bundesministerium für Bildung und Forschung and the Russian Ministry of Science and Technology is gratefully acknowledged. We also thank Forschungszentrum Jülich and JINR, Dubna for access to their facilities.

References

[1] Ledbetter H M 1985 *J. Mater. Sci.* **20** 2923
[2] Ledbetter H M and Kim S A 1988 *J. Mater. Sci.* **23** 2129
[3] Kim S A, Ledbetter H M and Li Y Y 1994 *J. Mater. Sci.* **29** 5462
[4] Beskrovni A, Danilkin S A, Fuess H, Jadrowski E L, Neova-Baeva M and Wieder T 1999 *J. Alloys Compounds* **291** 262
[5] Vitos L, Korzhavyi P A and Johansson B 2003 *Nat. Mater.* **2** 25
[6] Danilkin S A and Jadrowski E L 1997 *Physica* B **234** 900
[7] Danilkin S A, Fuess H, Wieder T and Hoser A 2001 *J. Mater. Sci.* **36** 811–4
[8] Hoelzel M, Danilkin S A, Hoser A, Ehrenberg H, Wieder T and Fuess H 2002 *Appl. Phys.* A **74** 1013
[9] Stassis C, Zaretsky J, Misemer D K, Skriver H L, Harmon B N and Nicklow R M 1983 *Phys. Rev.* B **27** 3303
[10] Stassis C, Loong C-K, Theisen C and Nicklow R M 1982 *Phys. Rev.* B **26** 4106
[11] Zaretsky J and Stassis C 1987 *Phys. Rev.* B **35** 4500
[12] Hallman E D and Brockhouse B N 1969 *Can. J. Phys.* **47** 1117
[13] Garg S, Gupta H C, Bansal T K and Tripathi B B 1985 *J. Phys. F: Met. Phys.* **15** 1895
[14] Kröner E 1958 *Z. Phys.* **151** 504
[15] Ledbetter H M 1981 *Br. J. Non-Destr. Test.* **34** 286
[16] Krebs K 1965 *Phys. Rev.* **138** A143
[17] Mohammed K, Shukla M M, Milstein F and Merz J L 1984 *Phys. Rev.* B **29** 3117
[18] Svensson E C, Brockhouse B N and Rowe J M 1967 *Phys. Rev.* **155** 619
[19] Birgeneau R J, Cordes J, Dolling G and Woods A D B 1964 *Phys. Rev.* **136** A1359
[20] Dawidowski J, Cuello G J, Koza M M, Blostein J J, Aurelio G, Fernández Guillermet A and Donato P G 2002 *Nucl. Instrum. Methods* B **195** 389
[21] Dawidowski J, Bermejo F J and Granada J R 1998 *Phys. Rev.* B **58** 706
[22] Gilat G and Raubenheimer L J 1966 *Phys. Rev.* **144** 390